Pergamon

Int. J. Heat Mass Transfer. Vol. 40, No. 3, pp. 641–655, 1997

0017–9310/97 $15.00+0.00

PII: S0017-9310(96)00104-4

Liquid-side interphase mass transfer in cocurrent vertical two-phase channel flows

D. LUO and S. M. GHIAASIAAN†

G. W. Woodruff School of Mechanical Engineering, Georgia Institute of Technology, Atlanta, GA 30382-0405, U.S.A.

(*Received* 30 *August* 1995 *and in final form* 15 *March* 1996)

Abstract—Volumetric liquid-side interphase mass transfer coefficients were experimentally measured in vertical channels supporting cocurrent, upward two-phase flows. Deionized water and an aqueous solution of sucrose constituted the liquid phase, pure nitrogen was the gas phase, and oxygen was the transferred species. In each test, oxygen concentrations in the liquid at two measurement stations near the two ends of the test section were measured on-line. The channel entrance effects were eliminated by performing hydrodynamically-identical tests with two different test section lengths, and using the shorter test section results for quantification of entrance effects in the longer test section. The channel average gas holdups representing developed flows were also measured using two simultaneous, quick-closing valves. The obtained data were compared with predictions of several widely-referenced correlations, with significant disagreements among the correlations, and between the correlations and the data. New empirical correlations were developed based on the obtained data representing the fully-developed slug and churn flow regimes. Copyright © 1996 Elsevier Science Ltd.

1. INTRODUCTION

Currently, the separated flow modeling is the most widely-used approach for the analysis of multi-phase flows, where the mixture is divided into a number of fluids, each is represented by a separate set of conservation equations, while mass, momentum, and energy exchanges among the fluids are quantified using appropriate closure relations. The two-fluid modeling technique is the basis of most major thermal-hydraulic codes for nuclear reactor accident analysis [1–4] and many recently-published mechanistic models [5–7]. Three-fluid models have also been recently developed [8–13]. Multi-fluid modeling requires detailed closure relations for interphase transfer processes. For the latter, the interfacial surface concentrations, and the associated transfer coefficients are needed. The available models and correlations are generally inadequate, however, and current computational techniques for numerical solutions of multi-fluid conservation equations are significantly more advance than the state-of-art associated with modeling of interphase transfer processes [14, 15]. The need to improve these methods is now well recognized.

The objective of this investigation was to experimentally measure the liquid-side interphase mass transfer coefficient in cocurrent, upward two-phase channel flows.

† Author to whom correspondence should be addressed.

2. REVIEW OF PREVIOUS STUDIES

2.1. *Experimental investigations*

Interfacial heat transfer data dealing with bubbly, slug and churn flow patterns are literally non-existent due to the difficulty of experimental measurement. Some mass transfer data at the gas–liquid interface exist. Most of the previous studies attempted to measure the interfacial specific area by the imposition of a fast chemical reaction in the liquid, and experimental data addressing interphase mass transfer without imposing a chemical reaction in the liquid are few. Several important studies, which have led to the development of correlations are listed in Table 1, and are briefly explained below.

In the experiments of Heuss *et al.* [16], the results were strongly affected by the entrance effects. Scott and Hayduk [17] used a small adjustable probe for extracting liquid samples at various depths in their test section. In the experiments of Lamont and Scott [18, 19] uniform sized spherical bubble streams were produced in the test section with frequencies of 100–1500 min^{-1}. They attributed the strong liquid-side controlled mass transfer coefficients to the surface renewal processes by turbulent eddies of sizes much smaller than the bubble diameters, and proposed a theory in which the motion of the eddies were idealized, and were assumed to occur in regular, two-dimensional (2D) cells. Jepsen [20] used two parallel 4.88 m long horizontal pipes connected together by a U bend. The transfer rate of oxygen was determined in his experiments by continuously withdrawing liquid

NOMENCLATURE

- a specific interphase area per unit mixture volume [m^{-1}]
- C_{He} Henry's coefficient [Nm^{-2}]
- C_1, C_2 dimensionless constants in Nicklin's correlation [equations (25) and (26)]
- d channel diameter [m]
- D molecular mass diffusivity [$m^2 s^{-1}$]
- Eu Euler number $= (\Delta P/L)d/\rho U^2$
- G mass flux [$kg m^{-2} s^{-1}$]
- g gravitational constant [$m s^{-2}$]
- k_L liquid-side mass transfer coefficient [$m s^{-1}$]
- L length [m]
- L' length of long test section [m]
- L'' length of short test section [m]
- M molecular mass [$kg kmol^{-1}$]
- m mass fraction
- n mass transfer rate per unit mixture volume [$kg m^{-3} s^{-1}$]
- P pressure [Nm^{-2}]
- Pe_L liquid-phase Peclet number $= U_{LS}d/D_L$
- Q volumetric flow rate [$m^3 s^{-1}$]
- Re_L liquid Reynolds number $= U_{LS}d/\nu_L$
- r first-order reaction velocity constant [s^{-1}]
- s fractional rate of surface renewal [s^{-1}]
- Sc_L liquid-phase Schmidt number $= \nu_L/D_L$
- Sh_L liquid-side Sherwood number $= k_L d/D_L$
- T temperature [K]
- V volume [m^3]
- V_{E1}, V_{E2} volumes of the entrance and exit segments of the test sections [m^3]
- V', V'' volumes of the long and short test sections, respectively [m^3]
- $U_{B,\infty}$ rise velocity of Taylor bubbles [$m s^{-1}$]
- U_{GS} gas superficial velocity (gas volumetric flow rate divided by cross-sectional area) [$m s^{-1}$]
- U_h homogeneous mixture velocity $= (\rho_L U_{LS} + \rho_G U_{GS})/(\rho_L(1-\alpha) + \rho_G\alpha)$ [$m s^{-1}$]
- U_{LS} liquid superficial velocity (liquid volumetric flow rate divided by cross-sectional area) ($m s^{-1}$)
- X mole fraction
- z axial coordination [m].

Greek letters

- α gas holdup
- δ thickness of stagnant fluid layer [m]
- ε rate of energy dissipation by turbulence per unit volume [Wm^{-3}]
- μ dynamic viscosity [$kg m^{-1} s^{-1}$]
- μ_L^* relative viscosity of liquid
- ν kinematic viscosity [$m^2 s^{-1}$]
- ρ density [$kg m^{-3}$]
- σ surface tension [$N m^{-1}$]
- τ surface renewal characteristic time [s].

Subscripts

- B bubble
- F friction
- G gas
- h homogeneous
- L liquid
- O_2 oxygen
- P pressure
- s S-surface
- S1, S2 measurement stations S1 and S2
- TP two-phase
- W water.

samples and determining their oxygen concentrations. The measured $k_L a$ values showed good agreement with the data of Scott and Hayduk [17] in low energy dissipation range, and were about 10 times lower than the data of Heuss *et al.* [16] at high energy dissipation rates. The discrepancy was attributed by Jepsen to the entrance effect in the experiments of Heuss *et al.*

Kasturi and Stepanek [22, 23] measured the interfacial surface area concentrations and the liquid- and gas-side mass transfer coefficients. The measured a and $k_L a$ values both monotonically increased with increasing U_{LS}. The dependence of a and $k_L a$ on U_{GS} was not monotonic, and both reached a maximum at $U_{GS} \approx 8$ m s^{-1}. In the experiments of Tomida *et al.* [24], $k_L a$ reached a maximum value when $U_{GS} \approx 4$ m s^{-1} at the lowest liquid velocity ($U_{LS} = 0.13$ m s^{-1}), but monotonically increased with gas velocity at higher liquid velocities ($U_{LS} > 0.35$ m s^{-1}).

Many investigators measured and/or correlated the specific interfacial area. Techniques for measurement of specific interfacial area include: photography; proton attenuation; ultrasonic methods; and most importantly electric probes [25–31], and absorption–desorption techniques [20, 22–24, 32–43]. Theses investigations thus far have not led to generally valid models or correlations.

In summary, the existing experimental data have the following shortcomings. (1) They are limited, and are in disagreement with each other. (2) The entrance effect has not been adequately eliminated or quantified in most of them. (3) Most of the data were obtained by using various sampling techniques. Errors can occur

Table 1. Previous experimental data

Source	Tomida *et al.* [24]	Jepsen [20]	Scott and Hayduk [17]	Heuss *et al.* [16]	Kasturi and Stepanek [22, 23]	Lamont and Scott [18]
Test section diameter [cm]	Vertical 1.0, 1.8, 2.5	Horizontal 2.54, 10.16	Horizontal 1.27, 1.78, 2.54	Horizontal 2.54	Vertical 0.6	Vertical and horizontal 0.79, 15.9
Test section length [m]	3.0, 4.0	9.76	2.34	1.35	1.5	4.27
Flow configuration	Cocurrent	Cocurrent	Cocurrent	Cocurrent	Cocurrent	Cocurrent
Gas phase	Air	Air	CO_2 and He	Air	Air	CO_2
Liquid phase	Water Water + glycerin Water + malt honey	Water	Water, ethanol, and ethylene glycol	Water	NaOH + water Na_2CO_3–$NaHCO_3$ + water	Water
Transferred species	CO_2	O_2	CO_2	O_2	SO_2, CO_2	CO_2
U_{GS} [m s^{-1}]	1.6–33	0.8–10.9† 11.9–48.8‡	0.03–6.1	4.3–15.2	1.1–11	0.00013–0.05
U_{LS} [m s^{-1}]	0.13–1.1	0.3–2.3† 1.3–3.6‡	0.15–1.1	2.1–4.9	0.07–0.5	0.1–2.5
Flow regime	Froth Wavy annular	Slug-churn† Annular‡	Bubbly Plug	Froth	Bubbly Slug-churn	Bubbly

† Tests with 2.54 cm i.d. tube.
‡ Tests with 10.16 cm i.d. tube.

because the sample gas can contain small droplets and the sample liquid can contain small bubbles. During the period the phases are allowed to separate in the sample, furthermore, mass transfer between the two phases continues, leading to uncontrolled errors.

2.2. *Models and correlations*

Models addressing interphase mass flux are many, and include the classical film model [44], penetration theory [45], and surface renewal theory [46]. Each of these models requires that a characteristic quantity, which mainly depends on the hydrodynamics (δ, τ and s, respectively) be specified. According to Danckwerts's model, when mass transfer is from gas to liquid and a very fast first-order chemical reaction between the transferred species and the liquid solution takes place, k_L is independent of s, and can be found from

$$k_L = \sqrt{D_L r}. \tag{1}$$

Consequently, in an experiment where the overall volumetric mass transfer rate is measured, the effective interfacial surface area concentration for mass transfer can be calculated. This approach has been applied by many investigators [22–34, 39–43].

Other widely-used modeling approaches include the introduction of an eddy diffusivity coefficient to account for the turbulent convective effects [47], and the idealization of turbulent eddy characteristics [19, 48–50]. Except for ref. [47], all of these models, in agreement to Levich's theory [51], predict:

$$K_L \propto \sqrt{D_L}. \tag{2}$$

Application of any of the above models evidently requires that the specific interfacial area and the details of turbulence in the liquid be known. A number of investigators have derived empirical and semi-analytical correlations. Several of these important investigations are reviewed below. The experiments were described in the previous section.

Heuss *et al.* [16] suggested:

$$Sh_L = 0.0316 Re^{0.9} \alpha^{-3.0} \quad (Re = U_h d/\nu_L). \tag{3}$$

Scott and Hayduk [17] correlated their data according to:

$$K_L a = 0.00688 U_{LS} \left(\frac{U_{GS}}{U_{GS}+U_{LS}}\right)^{0.774} \times \frac{\sigma^{0.511}\mu_L^{0.088} D_L^{0.390}}{d^{1.88}}. \tag{4}$$

In the above expression, velocities are in ft s^{-1}, surface tension in dyn cm^{-1}, viscosity in centipoise, diameter in cm, diffusion coefficient in $(cm^2\ s^{-1}) \times 10^5$, and $k_L a$ is in s^{-1}.

Jepsen [20] correlated his data according to:

$$K_L a = 3.47 \varepsilon^{0.4} \mu_L^{0.05} \sigma^{0.5} D_L^{0.5} d^{-0.68} \quad (\varepsilon < 0.05\ \text{atm s}^{-1}) \tag{5}$$

$$k_L a = 18.75 \varepsilon^{0.79} \mu_L^{0.05} \sigma^{0.05} D_L^{0.5} \quad (\varepsilon \geqslant 0.05\ \text{atm s}^{-1}) \tag{6}$$

$$\varepsilon = \left(\left|\frac{dP}{dz}\right|\right)_{TP,F} (U_{GS} + U_{LS}) \tag{7}$$

where

$$\left(\left|\frac{dP}{dz}\right|\right)_{TP,F}$$

is the two-phase flow frictional pressure gradient. The variables in the above equations have the same units as those in equation (4), and ε should be in atm s^{-1}.

Kasturi and Stepanek [22, 23] correlated k_L and a separately. Their correlation for a is [22]:

$$\frac{Q_L a}{1-\alpha} = 0.226 \left(\left|\frac{dP}{dz}\right|\right)_{TP,F}^{1.07} \tag{8}$$

where $Q_L a$ is in $cm^2\ s^{-1}$, and the frictional pressure gradient is in Nm^{-2}. Evidently the above correlation is specific to their experimental apparatus. They utilized equation (8) for their tests, and derived the following correlation for k_L, based on the analogy between momentum and mass transfer [23]:

$$Sh_L = 0.25 Sc_L^{0.5}\, Pe_L Eu_L \tag{9}$$

where Eu_L is defined as

$$\left(\left|\frac{dP}{dz}\right|\right)_{TP,F} d/\rho_L U_{LS}^2.$$

A correlation by Tomida *et al.* [24], also based on mass and momentum transfer analogy, is:

$$\frac{Sh_L(ad)}{Eu_L Sc_L^{0.5} Re_L (\mu_L/\mu_W)^{1.7}\alpha} = 7 \times 10^{-8} Re_L^2 + 0.0035 \quad (Re_L \leqslant 1500) \tag{10}$$

$$\frac{Sh_L(ad)}{Eu_L Sc_L^{0.5} Re_L (\mu_L/\mu_W)^{1.7}\alpha} = 10^{-4} Re_L \quad (Re_L > 1500) \tag{11}$$

where now

$$Eu_L = \left(\left|\frac{dP}{dz}\right|\right)_{TP} d/\rho_L U_{LS}^2, \text{ with } \left(\left|\frac{dP}{dz}\right|\right)_{TP}$$

representing the total pressure gradient. Tomida *et al.* [40] subsequently performed mass transfer experiments by absorbing oxygen into sodium sulphite solutions, and measuring the parameter a. They applied hypothermic syringes for sampling. Combining the latter data with the aforementioned correlations for $k_L a$ [equations (10) and (11)], Tomida *et al.* [40] also derived independent correlations for k_L.

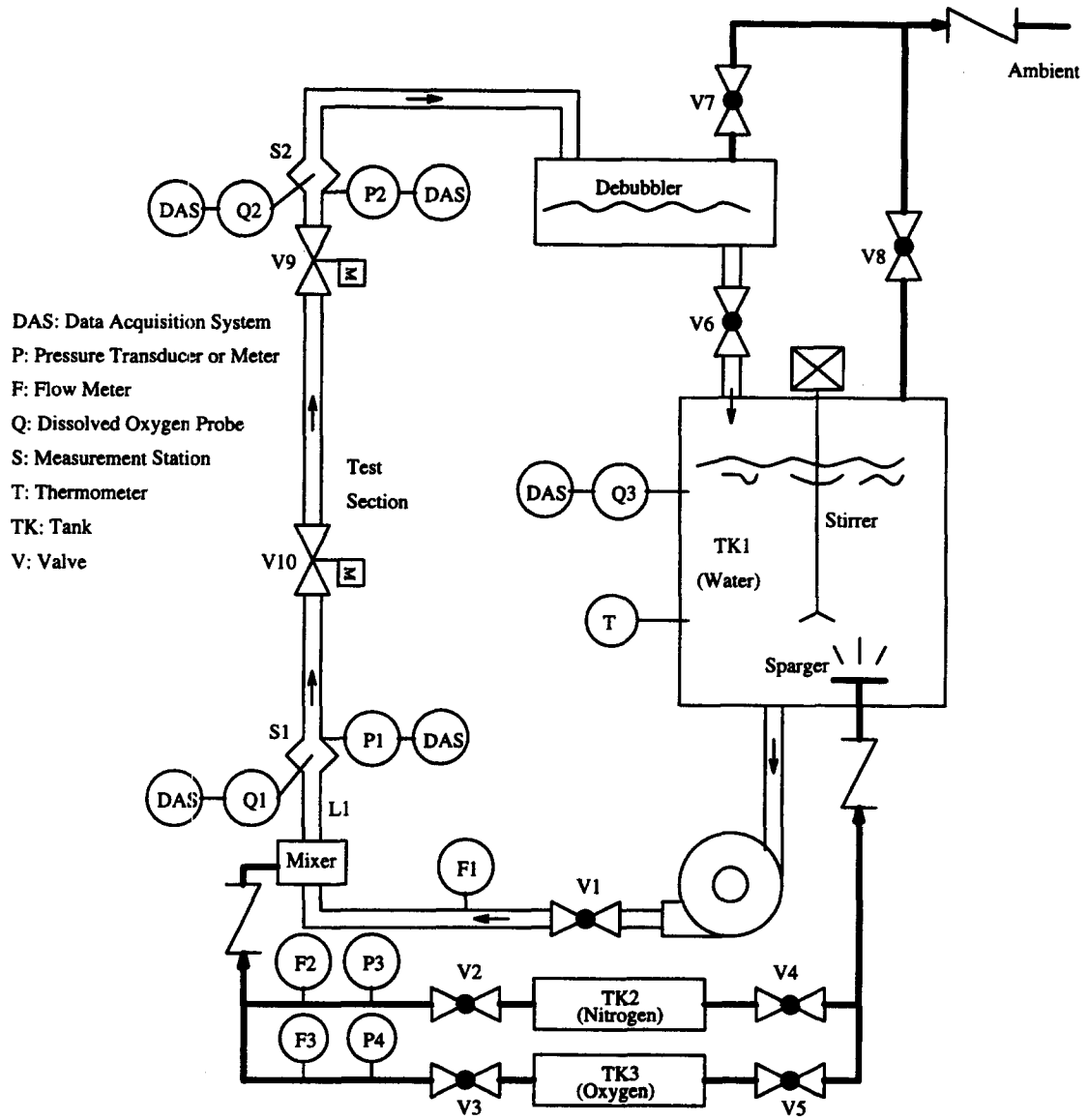

Fig. 1. Schematic of the test facility.

3. EXPERIMENTS

3.1. *Test facility*

Figure 1 is a schematic of the test facility. The major components include the main water tank (TK1), the nitrogen tank (TK2), the oxygen tank (TK3), the mixer, the water pump, the debubbler, and the test section. All the depicted valves except those used on flow meters were PVC ball valves, and all piping connections were made of PVC or Plexiglas. Needle valves were used for adjusting liquid and gas flow rates. Nitrogen flow is adjusted by valve V2 before entering the mixer. From the mixer, the gas–liquid mixture flows through the tube segment L1 (38.1 cm long and 5.08 cm i.d.) before reaching the measurement station S1. Tank TK1 is made of transparent plexiglas sheets and is 0.68 m × 0.70 m × 1.22 m in dimension. It is provided with a stirrer, a thermometer, a dissolved oxygen probe and a gas sparger. The oxygen concentration of the liquid inside the tank can be adjusted by sparging either nitrogen to deoxygenate the liquid, or oxygen to raise its oxygen concentration.

The test sections are transparent vertical tubes, made of plexiglas. Two different tubes, 1.9 cm and 5.08 cm i.d., are used. The test sections also have two different lengths, 3.31 m and 1.54 m. Hydrodynamically identical tests (i.e. tests with identical inlet gas and liquid flow rates) are performed with these two test section lengths, and the results of shorter test section are used to quantify the entrance effects in the longer test sections. Valve V9 and V10 are normally-open quick-action solenoid valves, 1.9 m apart, and are used for measuring the average gas holdup in the developed flow segment of longer test

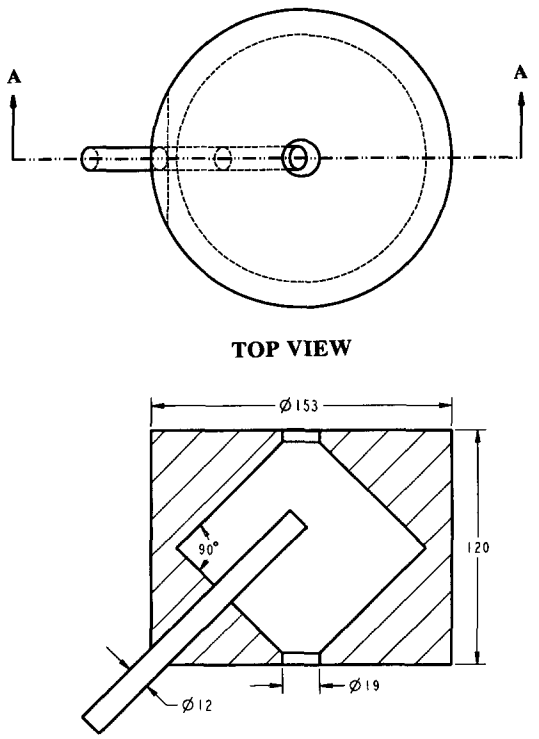

Fig. 2. Configuration of ion-selective electrodes in measurement station S1 (all dimensions are in mm).

section. When power is turned on via a common switch, the solenoid valves quickly and simultaneously cut off the flow.

Measurement stations S1 and S2 are each a combination of a converging and diverging cone with 90° apex angle, as depicted in Fig. 2. They were constructed by machining Plexiglas blocks. Details of the machined block are shown in Fig. 2 for one station (Station S1 with smaller test section) only. Others were similar. An ion-selective electrode (1.2 cm diameter) for on line reading of oxygen concentration in water is installed in each sampling station. The electrode tips are located on the channel axis. The probes' tips are equipped with membranes sensitive to oxygen, and it is crucial to prevent bubbles from adhering to these membranes. With the designs depicted in Fig. 2, bubble-membrane attachment was not observed during experiments. The relatively large size of the probes, and the vigorous mixing observations in the measurement stations support the assumption that the probes measured the averaged oxygen concentrations. Back mixing, in particular in tests with very low liquid superficial velocities, occurred in the measurement stations. Since only time-averaged oxygen concentrations are measured (see Section 3.3), back mixing of liquids poses no problem. It is also conceivable that some microbubbles may collide and contact with the oxygen probes due to back mixing, However, the method used for eliminating the test section end effects, to be described later, effectively eliminates the influence of these microbubbles.

The mixer is a vertical cylinder 12.7 cm in diameter and 15 cm in height. Gas is injected into the mixer through two mutually perpendicular porous cylinders, each 2 cm in diameter and 12.7 long, with 0.8 mm pore size. The debubbler is a horizontal vessel 1.19 m long, 0.32 m wide and 0.46 m high. The long residence time of the mixture in this vessel provides for phase separation, whereby the gas is discarded to the ambient, and water returns to the main water tank.

3.2. *Instrumentation and data acquisition*

Figure 1 also depicts the major measurement instruments. The dissolved oxygen probes are model 97-08 oxygen electrodes made by Orion Research, Inc. (Boston, MA). Together with the data acquisition system, they provide on-line dissolved concentration measurements. The measurement range is from 0 to 14 ppm and the accuracy is 0.05 ppm or 2%, whichever is greater, between 15 and 35°C, with the temperature of the air (used for calibration) within 10°C of the sample temperature. The response time is 96% response in less than 30 s between oxygen free and air-saturated water at 22°C. The oxygen probes were calibrated once every hour of exposure, in water saturated with air. The oxygen concentration in this water sample was measured by a YSI Model 50B (YSI Inc., Yellow Springs, OH) dissolved oxygen meter. The accuracy of the meter is 0.7%. The meter itself was calibrated in water saturated with air, according to the calibration table provided by the aforementioned manufacturer.

The present transducers (Model SA, Data Instruments Inc., Acton, MD) measured the absolute pressures in the 0–690 kPa range, and the accuracy of measurement is 1% span from best fit straight line. The water flow rate was measured by block-type flowmeters (King Instrument Company, Huntington Beach, CA). The gas flow rates were measured using a flowmeter system composed of a frame with flow adjusting valves and flow tubes (Cole-Palmer Flowmeter Component System). The viscosity of the sucrose solution was measured by using the Cannon-Fenske Routine Viscometer provided by Fisher Scientific. The precision of the viscometer is 0.2%. The viscometer was cleaned by acid, distilled water and acetone before every measurement. All these instruments were calibrated during the experiments, as detailed in ref. [55].

3.3. *Experimental procedures*

The procedure for mass transfer experiments includes the following steps:

(1) Adjustment of the liquid properties and oxygen concentration in the main water tank TK1. The oxygen concentration in the tank was maintained higher than 6 ppm by sparging oxygen through it, in order to avoid excessive experimental uncertainties.

(2) Calibration of instruments. The oxygen probe and pressure transducers were calibrated before each test series representing a constant liquid flow rate while gas flow rate was changed (14 data points, taken in about 45 min).

(3) Establishment of desired two-phase flow. This was done by first adjusting the water flow rate in the test section, and then introducing nitrogen into the mixer.

(4) Variation of flow rates. The gas flow rate was systematically varied while maintaining the liquid flow rate constant.

During each data recording, the signals from the oxygen probes were collected ten times, approximately at one second intervals, and averaged. The measured oxygen concentrations were thus ensemble-averaged quantities, and due to the large number of measurements are assumed to represent time-averaged quantities. For convenience, the gas hold-up tests were performed in separate purely hydrodynamic experiments, without mass transfer. These tests, however, duplicated the hydrodynamic conditions of the mass transfer experiments. Each experiment was repeated three times in order to examine repeatability.

3.3.1. *Properties.* The solubility and molecular diffusivity of oxygen in water are easily available [52]. Important properties of sucrose solutions have been studied by Hikita *et al.* [53], who measured the densities and dynamic viscosities of aqueous sucrose solutions, as functions of temperature and sucrose concentration. They also determined the diffusivities of oxygen in aqueous sucrose solutions by measuring the rates of absorption of oxygen in a wetted-wall column. They derived the following simple relation, which predicted their data, in the $0 \leqslant \mu_L^* \leqslant 30$ and 14–43°C range, with an average deviation of only 4.2%.

$$\frac{D_L}{D_W} = \left(\frac{\mu_L}{\mu_W}\right)^{-2/3}. \tag{12}$$

The sucrose solution concentration used in this study was constant, at 25% by weight (25 g of sucrose added to 75 g of water). The mixture density was 1119 kg m^{-3} everywhere, which was directly measured. The viscosity of the sucrose solution, as a function of temperature was also measured, and μ_L^* was about 2.55 in all tests. In view of equation (12), Sc_L was approximately four times larger in the sucrose solution than in pure water. Dissolved sucrose has a very small effect on water surface tension [54]. Using a tensiometer, the surface tension of 25% sucrose solution was measured in this study, and compared with the surface tension of pure water with negligible difference.

3.3.2. *Data analysis.* The mass transfer data are analysed assuming: (1) the liquid is well mixed at any location along the test section; (2) the mass transfer process is liquid-side controlled, and the gas-phase mass transfer resistance can be neglected and (3) the effects of measurement stations S1 and S2 can be lumped into an effective, volume-averaged k_La for the test section. Although according to the last assumption mass transfer in measurement stations is included in the defined k_La values, the method used for eliminating the channel end effects, to be described below, effectively removes the impact of this assumption. Due to the small solubility of oxygen in water, U_{LS} and U_{GS} remain approximately constant and the liquid- and gas-side oxygen species conservation can be represented as:

$$\rho_L U_{LS} \frac{d}{dz} m_{O_2,L} = -n_{O_2} \tag{13}$$

$$\rho_G U_{GS} \frac{d}{dz} m_{O_2,G} = n_{O_2} \tag{14}$$

where

$$n_{O_2} = (k_La)(m_{O_2,L} - m_{O_2,u})\rho_L \tag{15}$$

$$m_{O_2,u} = \frac{X_{O_2,u} M_{O_2}}{X_{O_2,u} M_{O_2} + (1.0 - X_{O_2,u}) M_{H_2O}} \approx X_{O_2,u} \frac{M_{O_2}}{M_{H_2O}} \tag{16}$$

$$X_{O_2,u} = \frac{P X_{O_2,G}}{C_{He,O_2}} \tag{17}$$

$$X_{O_2,G} = X_{O_2,G|S1} + \frac{\rho_L U_{LS} (m_{O_2,L|S1} - m_{O_2,L}) M_G}{\rho_G U_{GS} M_{O_2}}. \tag{18}$$

In equation (17), P is the local pressure, which is found from

$$P = P|_{S1} + \frac{P|_{S2} - P|_{S1}}{L} z. \tag{19}$$

For each data point, a value for k_La was assumed, and equations (13) and (14) were integrated along the test section using measured values of m_{O_2L} and P at measurement station S1 as the initial conditions. Iterative integrations, using k_La as the parameter, were repeated until the calculated value of m_{O_2L} at S2 matched the measured value. Once the k_La values for the long test section ($L' = 3.31$ m) and short test section ($L'' = 1.54$ m) were obtained for identical flow parameters, the fully-developed k_La values without the effect of test section entrance and exit were calculated. To derive the necessary relation for this purpose, the following assumptions are made: (1) the shorter test section is sufficiently long to represent both entrance and exit effects of the longer test section; and (2) the two phase flow regime in the shorter test section is identical to the flow regime in the entrance and exit segments of the longer channel. The time and volume-averaged volumetric mass transfer coefficients for the long and short channels are accordingly defined as:

$$(k_La)_{L'} AL' = \int_{V_{E1}} k_La \, dV + \int_{V_{E2}} k_La \, dV + \int_{V' - (V_{E1} + V_{E2})} k_La \, dV \tag{20}$$

$$(k_La)_{L''}AL'' = \int_{V_{E1}} k_La\,dV + \int_{V_{E2}} k_La\,dV + \int_{V''-(V_{E1}+V_{E2})} k_La\,dV. \quad (21)$$

Note that in writing the above two equations no assumptions other than the aforementioned assumptions 1 and 2 have been made. The total time-averaged volumetric mass transfer coefficient in the developed segment of the long channel can now be obtained by subtracting equation (21) from equation (20), and since the developed channel segment is cylindrical, there results:

$$k_La = \frac{(k_La)_{L'}L' + (k_La)_{L''}L''}{L' - L''}. \quad (22)$$

A necessary precaution in mass transfer experiments similar to this investigation is to avoid equilibrium in the test section. Neglecting the accumulation of oxygen in the gas phase, the oxygen mass fraction in the liquid leaving the longer test section can be found from

$$\frac{m_{O_2,L}(L')}{m_{O_2,L|_{SI}}} = \exp\left[-\frac{(k_La)_{L'}L'}{U_{LS}}\right]. \quad (23)$$

In the experiments, typically

$$\frac{(k_La)_{L'}L'}{U_{LS}} < 2$$

and the maximum value was about 3.2.

3.4. *Uncertainties*

Experimental uncertainties for the fully-developed k_La values due to random measurement errors were calculated assuming that the accuracy of each measured k_La value was affected by the accuracy of the oxygen probes, flow meters, pressure transducers, and temperature measurements. The accuracy of the fully-developed k_La values is also affected by the data scatter representing measured k_La values for the long and short test sections. Details of the uncertainty analysis can be found in Luo [55].

4. EXPERIMENTAL RESULTS

4.1. *Flow regimes and gas hold-up*

The experiments covered the following superficial gas and liquid velocity ranges. For the 1.9 cm inner diameter test section, $0.1\ \text{m s}^{-1} \leqslant U_{LS} \leqslant 1.5\ \text{m s}^{-1}$ and $0.1\ \text{m s}^{-1} \leqslant U_{GS} \leqslant 7.5\ \text{m s}^{-1}$ were used. For the 5.08 cm inner diameter test section, due to the limited capacity of the gas injection system, the flow ranges were $0.1\ \text{m s}^{-1} \leqslant U_{LS} \leqslant 0.75\ \text{m s}^{-1}$ and $0.012\ \text{m s}^{-1} \leqslant U_{GS} \leqslant 0.95\ \text{m s}^{-1}$.

Figure 3(a) depicts the observed flow regimes in the 1.9 cm diameter test section with deionized water, where they are compared with predictions of the flow regime models of Taitel *et al.* [21]. Flow regimes with

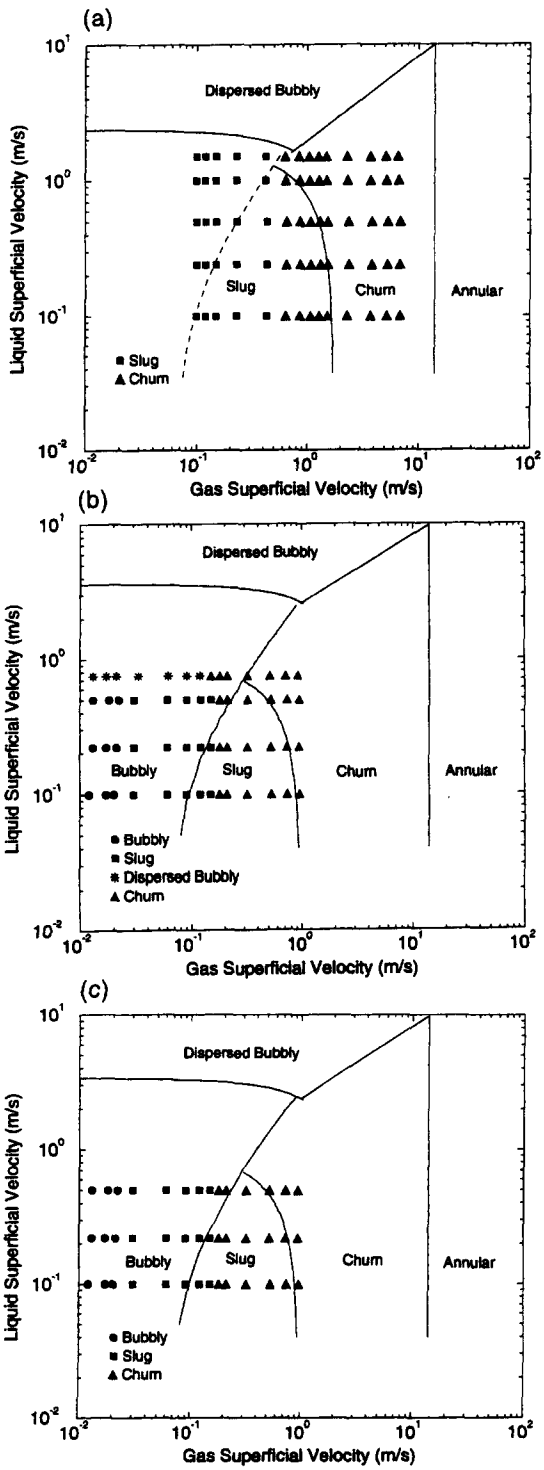

Fig. 3. Comparison between the experimental flow regimes and the Taitel *et al.* [21] flow regime models. (a) $d = 1.9$ cm, deionized water; (b) $d = 5.08$ cm, deionized water; (c) $d = 5.08$ cm, sucrose solution.

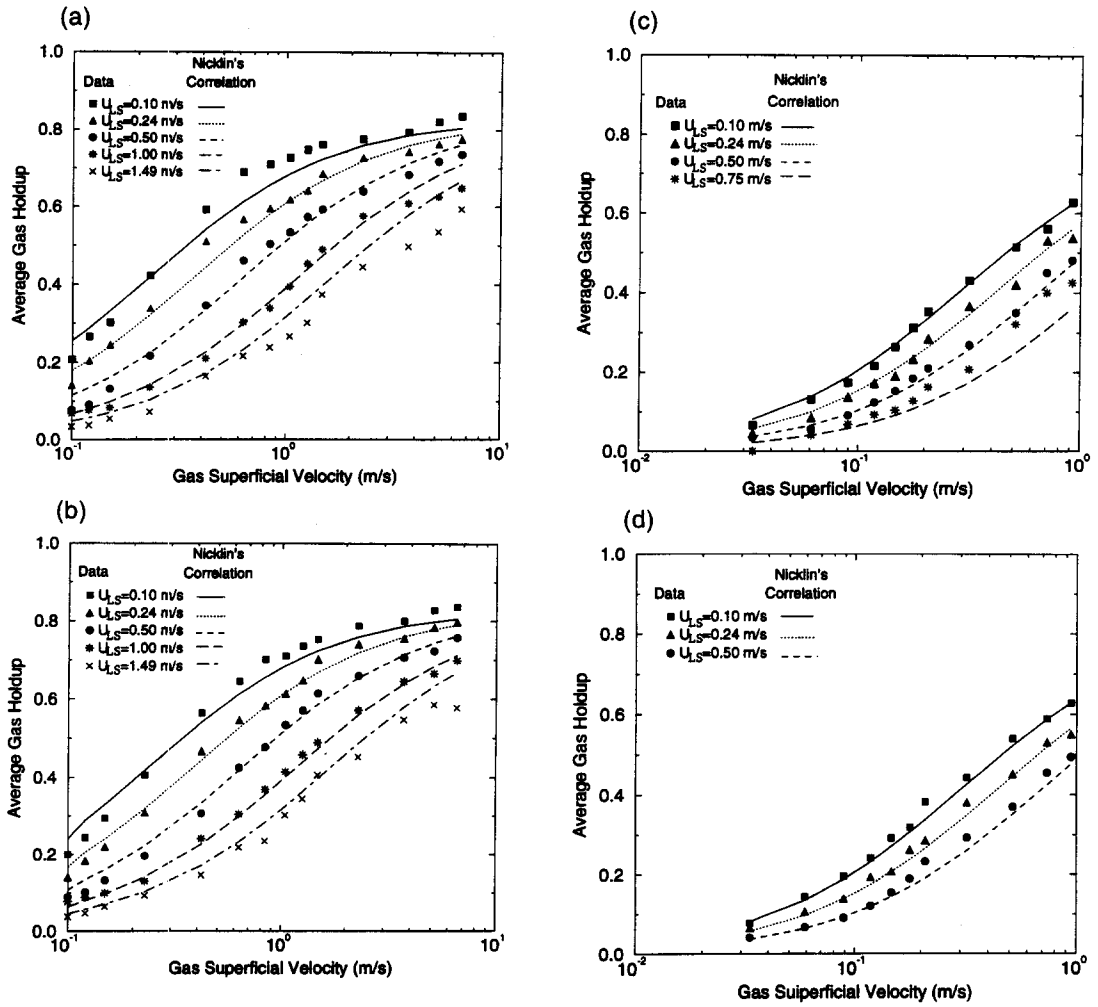

Fig. 4. Channel average gas hold-ups. (a) $d = 1.9$ cm, deionized water; (b) $d = 1.9$ cm, sucrose solution; (c) $d = 5.08$ cm, deionized water; (d) $d = 5.08$ cm, sucrose solution.

sucrose solution were very similar to Fig. 3(a). Bubbly flow does not occur in channels with $d \leqslant 5$ cm with air and water and the sucrose solution [21]. As noted, the data points are mostly in the slug and churn flow regions. Also, as noted, there is a relatively poor agreement between the data and the flow regime model of Taitel *et al.* [21] with respect to the border between slug and churn flow patterns. The flow regimes observed in the 5.08 cm i.d. test sections are displayed in Figs. 3(b) and 3(c), and include data in the bubbly flow regime.

Figures 4(a)–(d) depict the measured channel average gas holdups (*in situ* volume fraction of gas). An empirical correlation for gas holdup, suitable for the slug flow regime in vertical channels, was proposed by Nicklin *et al.* [56], and has been found to well-predict cocurrent flow [57, 58], as well as countercurrent flow data [59]:

$$\alpha = \frac{U_{GS}}{C_1(U_{GS}+U_{LS})+U_{B,\infty}} \tag{24}$$

where

$$C_1 = 1.2 \tag{25}$$

$$U_{B,\infty} = C_2\sqrt{gd}. \tag{26}$$

According to Martin [60], furthermore,

$$C_2 = 0.35. \tag{27}$$

Predictions of Nicklin *et al.*'s correlation, along with the above constants, are compared with our experimental data in Figs. 4(a)–(d). The correlation reasonably agrees with the data in both slug and churn flow regimes.

4.2. *Mass transfer*

Typical experimentally-measured k_La data, obtained in tests with the 1.9 cm diameter test sections with deionized water, are shown in Figs. 5(a)–(c). In each figure, the values of k_La for the short test section ($L'' = 1.54$ m), the long test section ($L' = 3.31$ m), and the developed flow obtained from equation (22) are all shown. In addition, the visually observed flow regimes are specified in the figures. Typical exper-

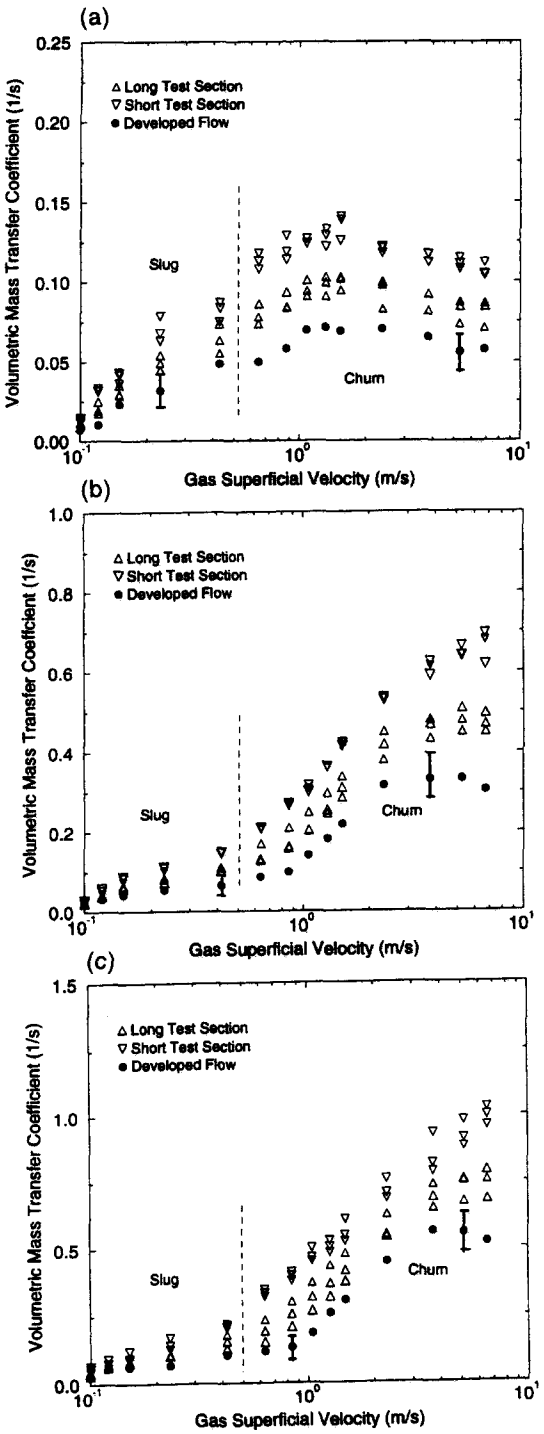

Fig. 5. Liquid-side volumetric mass transfer coefficients in tests with the 1.9 cm i.d. test sections, with deionized water. (a) $U_{LS} = 0.24$ m s^{-1}; (b) $U_{LS} = 1.0$ m s^{-1}; (c) $U_{LS} = 1.49$ m s^{-1}.

imental uncertainty bands are also provided for the developed flow data.

As noted, for both short and long test sections the k_La values are considerably higher than those for the developed flow. Entrance effects were significant in all tests. These figures also show that k_La monotonically increases as the liquid superficial velocity, U_{LS}, is increased. The dependence of k_La and U_{GS} is complicated and is influenced by the two-phase flow regime. Generally, at low U_{GS} where the flow regime is predominantly slug and the gas hold-up is sensitive to, and increases with increasing U_{GS}, the interfacial surface area, a, and possibly k_L, increase with increasing U_{GS}. At high U_{GS}, representing the high gas holdup churn regime, increasing U_{GS} may result in a reduction in the interfacial surface concentration, a, leading to a slightly downward trend in the k_La vs U_{GS} data. This downward trend was observed in most of the tests with the 1.9 cm i.d. test section, and appeared to be a characteristic of the churn flow regime, as the churn-to-annular regime transition is approached.

Figures 6(a) and (b) depict typical k_La data obtained with the 5.08 cm i.d. test sections, with sucrose solution, and confirm the significance of channel entrance effects. The 5.08 cm i.d. test section can support the bubbly flow regime [21], where due to the small gas hold-ups the measured k_La values are very

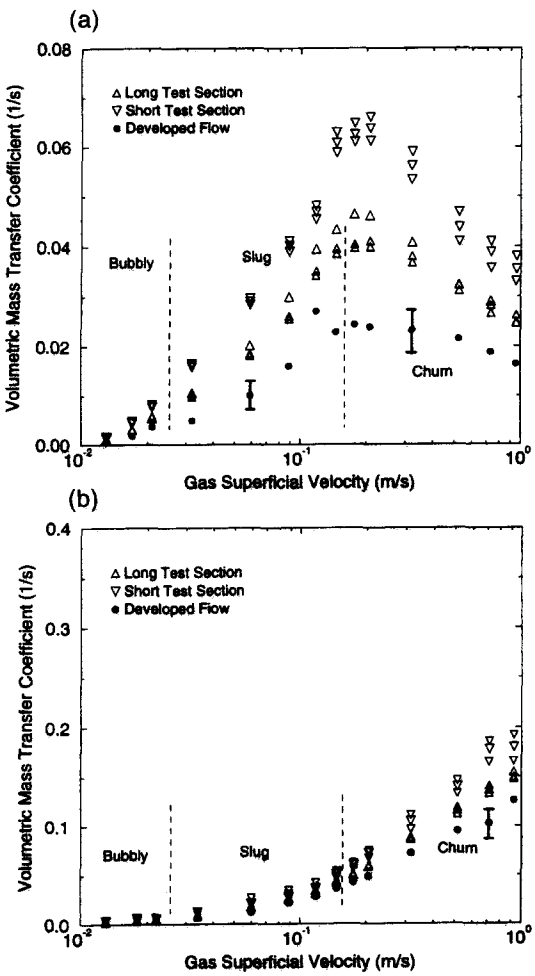

Fig. 6. Liquid-side volumetric mass transfer coefficients in tests with the 5.08 cm i.d. test sections, with sucrose solution. (a) $U_{LS} = 0.10$ m s^{-1}; (b) $U_{LS} = 0.5$ m s^{-1}.

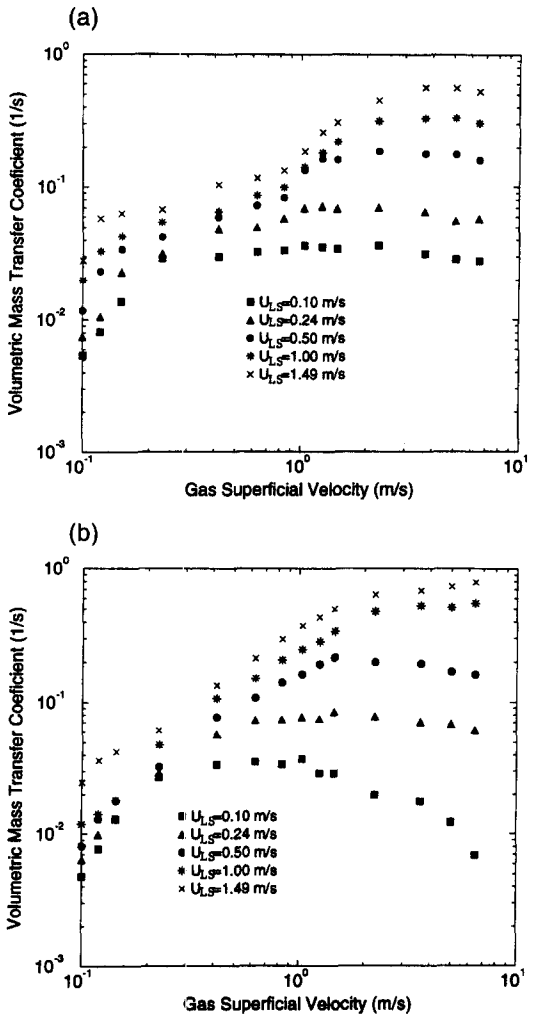

Fig. 7. Fully-developed liquid-side volumetric mass transfer coefficient in tests with the 1.9 cm i.d. test sections, the effects of liquid and gas superficial velocities: (a) deionized water; (b) sucrose solution.

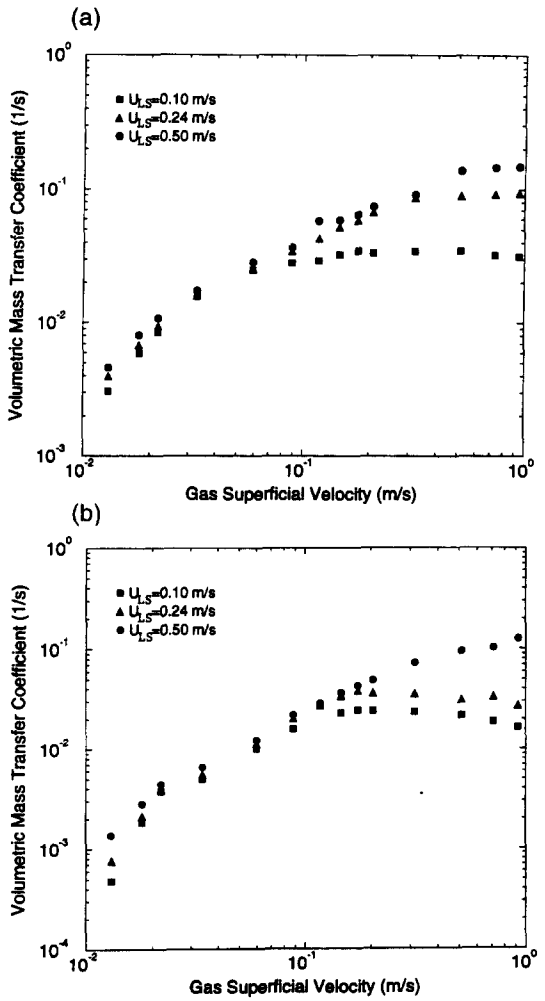

Fig. 8. Fully-developed liquid-side volumetric mass transfer coefficients in tests with the 5.08 cm i.d. test sections, the effects of liquid and gas superficial velocities: (a) deionized water; (b) sucrose solution.

small. The overall data trends are also similar, and indicate monotonically increasing k_La with U_{LS}. The data with 5.08 cm i.d. test sections, however, mostly indicate monotonically increasing k_La with U_{GS} and due to low gas superficial velocities the flow regime representing transition between churn and annular-dispersed regimes was not approached.

Figures 7 and 8 summarize the effects of U_{GS} and U_{LS} on the fully-developed k_La data. When compared to each other, furthermore, these figures represent various other parametric effects. As noted, k_La monotonically increases as U_{LS} is increased. It also monotonically increases with increasing U_{GS} in the bubbly, slug and part of the churn regimes, reaches a maximum in the latter flow regime, and slightly decreases as U_{GS} is increased in the range of U_{GS} where the transition from the churn to annular-dispersed flow patterns is approached. This downward trend can be observed in Figs. 7 and 8.

Comparison between Figs. 7(a) and (b), and

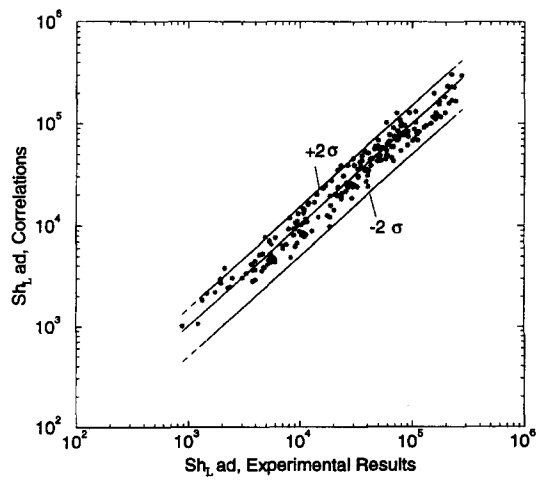

Fig. 9. Comparison of the fully-developed mass transfer data obtained from deionized water and sucrose solution experiments with the developed correlations.

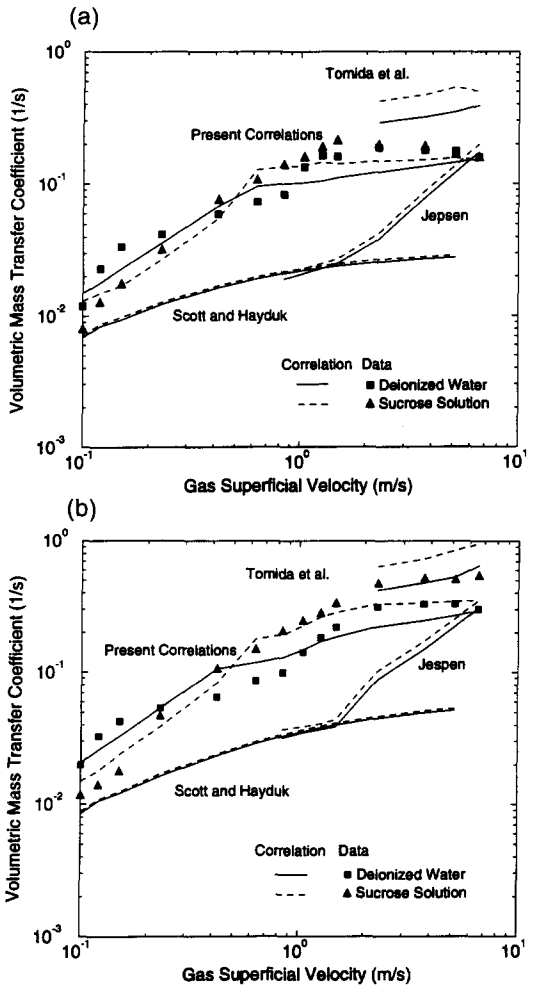

Fig. 10. Comparison of the fully-developed mass transfer data obtained from deionized water and sucrose solution experiments in the 1.9 cm i.d. tests sections with the correlations. (a) $U_{LS} = 0.5$ m s^{-1}; (b) $U_{LS} = 1.0$ m s^{-1}.

between Figs. 8(a) and (b), reveals the effect of Sc_L on the interphase mass transfer. (Note that $2040 \leqslant Sc_L \leqslant 2560$ for sucrose solutions, and $430 \leqslant Sc_L \leqslant 540$ for water in the tests. These variations were due to variations in laboratory temperature. Thus Sc_L is approximately four times larger for sucrose solution.) For the 1.9 cm i.d. test section, for $U_{GS} < 0.3$ m s^{-1}, representing the predominantly slug flow regime data, lower k_La values were obtained with the sucrose solution. In the churn flow regime, where $U_{GS} > 0.3$ m s^{-1}, tests with sucrose solution resulted in higher k_La values, except for the tests with $U_{LS} = 0.1$ m s^{-1}, where the trend was opposite. For the 5.08 cm i.d. test section the sucrose solution consistently provided lower k_La values.

4.3. *Correlation of the data and comparison with previous correlations*

The data obtained represent 238 fully developed flow data points, covering bubbly, slug and churn flow regimes. Out of these, 25 points represent bubbly or dispersed bubbly regimes. Since the mass transfer data trends are flow regime-dependent, separate empirical correlations should be developed for each flow regime. An effort was thus made to develop separate empirical correlations for the slug and churn flow patterns. Development of correlations for the bubbly and the dispersed bubbly flow regimes was not feasible due to the small number of these data points.

As discussed earlier, theory and previous experimental data indicate that $k_L \propto \sqrt{D_L}$, irrespective of the flow regime. The effect of mass diffusivity in the correlations is thus included according to the aforementioned relation. Other flow and property parameters were included in relevant dimensionless numbers. Analysis of the data led to the following correlations. For slug flow:

$$Sh_L ad = 3.16 \times 10^{-6} Sc_L^{0.5} (\mu_L^*)^{0.83} \times Eu_L^{0.44} Re_L^{0.87} \alpha^{-0.58} Re_G^{1.72}. \quad (28)$$

For churn flow:

$$Sh_L ad = 3.86 \times 10^{-4} Sc_L^{0.5} (\mu_L^*)^{1.68} \times Eu_L^{0.40} Re_L^{1.89} \alpha^{1.38} Re_L^{-0.20} \quad (29)$$

where $Eu_L = |dP/dz|_{TP}(\rho_L U_{LS}^2)^{-1}$, and is defined based on the total pressure gradient [24]. These correlations are based on the entire 213 relevant, fully-developed data points representing slug and churn-turbulent flow regimes obtained in this study, and represent the following ranges of parameters:

Deionized water: liquid superficial velocity: 0.10–1.49 m s^{-1}; gas superficial velocity: 0.012–7.5 m s^{-1}; liquid Reynolds number: 2180–44 000; gas Reynolds number: 40–8000; liquid-side Schmidt number: 430–540; channel averaged gas holdup: 0.043–0.83.

Sucrose solution: liquid superficial velocity: 0.10–1.49 m s^{-1}; gas superficial velocity: 0.012–7.5 m s^{-1}; liquid Reynolds number: 850–12 800; gas Reynolds number: 40–8000; liquid-side Schmidt number: 2040–2560; channel average gas holdup: 0.077–0.82.

Figure 9 compares the predictions of the above correlations with the experimental data. The correlation predicts the data, with a standard deviation of 25.2%.

Typical comparisons among the data and correlations obtained in this study, and previous correlations, are provided in Figs. 10(a) and (b) and 11(a) and (b). The sharp changes in the predictions of the present correlation are due to the change in the flow regimes, from slug to churn. In each figure only those correlations whose ranges of validity have an overlap with the depicted data are shown. The correlations of Jepsen [20], and Scott and Hayduk [17], which are based on data obtained in horizontal channels, are applied only where the mixture velocity is at least an order of magnitude larger than typical bubble rise velocities. The empirical correlations of Heuss [16] and Kasturi and Stepanek [22, 23] are not depicted,

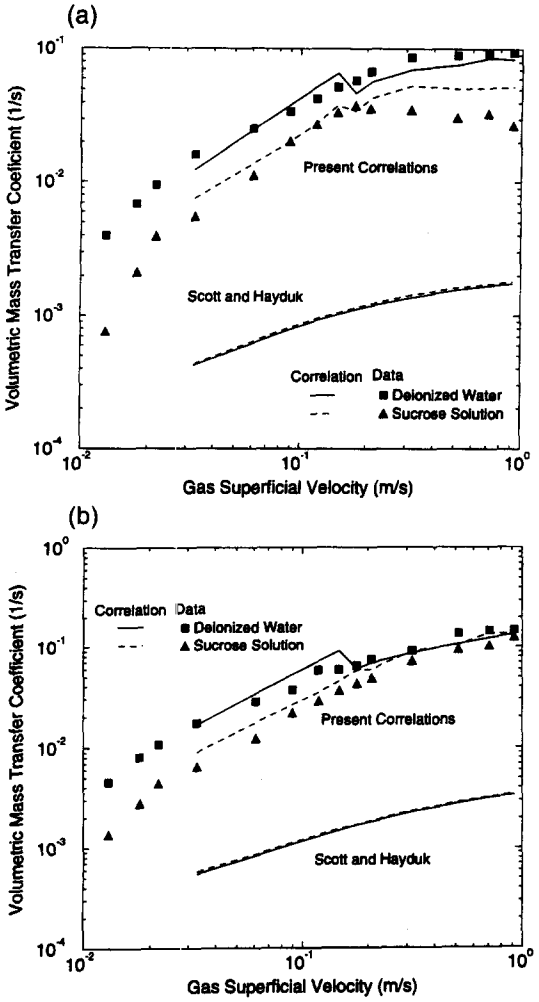

Fig. 11. Comparison of the fully-developed mass transfer data obtained from deionized water and sucrose solution experiments in the 5.08 i.d. test sections with the correlations. (a) $U_{LS} = 0.24\ m\ s^{-1}$; (b) $U_{LS} = 0.5\ m\ s^{-1}$.

since they are in terms of k_L, and their application would require a separate correlation for the interphase surface area concentration. The correlation of Scott and Hayduk [17] underpredicts the data by an order of magnitude and, in disagreement with the data, suggests a negligible effect of liquid viscosity on k_La. The correlations of Tomida *et al.* [24], on the other hand, systematically overpredict the data, typically by a factor of 2–4. Jepsen's correlation [20] is in fair agreement with the data at very high U_{GS} values, with respect to the predicted magnitudes of k_La. However, the latter correlation also underpredicts the data at lower gas superficial velocities, and predicts that k_La monotonically, and strongly, increases with increasing U_{GS}, in disagreement with the data. Evidently none of these correlations agree with the present experimental data.

5. CONCLUDING REMARKS

The liquid-side mass transfer in cocurrent, upward vertical channel flows was experimentally studied. Channels with 1.9 cm and 5.08 cm i.d. were used. In the experiments, all of which were performed at room temperature and at near-atmospheric pressure, the overall volumetric liquid-side mass transfer coefficients at the gas–liquid interphase, were experimentally measured. Water and 25% weight aqueous solution of sucrose (25 g sucrose dissolved in 75 g water) constituted the liquid phase, nitrogen was the gas phase, oxygen was the transferred species. Using dissolved oxygen probes, the oxygen mass fractions in the liquid at two stations near the two ends of the test sections were measured on line in the experiments, thus eliminating the possibility of systematic errors associated with the commonly-applied sampling techniques. The channel entrance effects were eliminated by performing hydrodynamically-identical tests (i.e. tests with the same liquid and gas flow rates) with two different test section lengths, 1.54 m and 3.31 m, and using the shorter test section results to quantify the entrance effects in the longer test section.

The data were compared with the previously-published correlations, generally with poor agreement between the data and each one of the correlations, and among the correlations themselves. These correlations, and the experimental data on which they are based, appear to bear the effects of systematic errors, due to channel entrance effects, and more importantly, due to errors associated with sampling techniques which were generally used in the experiments. New empirical correlations were developed separately for slug and churn regimes, which predict the volumetric mass transfer coefficient data with a standard deviation of 25.2%.

REFERENCES

1. D. D. Taylor *et al.* (9 authors), TRAC-BD1/MOD1 : An advanced best-estimate computer program for boiling water reactor transient, U.S. Nuclear Regulatory Commission Report, NUGREG/CR-3633 (1984).
2. V. H. Ransom *et al.* (7 authors), RELAP5/MOD2 code manual, U.S. Nuclear Regulatory Commission Report NUREG/CR-4312 (1985).
3. E. Carlson *et al.* (5 authors), RELAP5/MOD3 code manual, volumes I, II, III (draft), U.S. Nuclear Regulatory Commission Report, NUREG/CR-5535 (1990).
4. K. O. Passamehmetoglu *et al.* (14 authors), TRAC-PF1/MOD2 theory manual, U.S. Nuclear Regulatory Commission Report (draft) (1990).
5. T. Siikonen, Numerical method for one-dimensional two-phase flow, *Numer. Heat Transfer* **12**, 1–18 (1987).
6. G. F. Hewitt and A. H. Govan, Phenomenological modeling of non-equilibrium flow with phase change, *Int. J. Heat Mass Transfer* **33**, 229–242 (1990).
7. S. M. Ghiaasiaan, B. K. Kamboj and S. I. Abdel-Khalik, Two-fluid modeling of condensation in the presence of noncondensables in two-phase channel flow, *Nucl. Sci. Engng* **119**, 1–17 (1995).
8. W. H. Amarasooriya and T. G. Theofanous, Premixing of steam explosions : a three-fluid model, *Proceedings of the 25th National Heat Transfer Conf.*, Houston, TX, pp. 191–200 (1988).
9. D. F. Fletcher, An improved mathematical model of melt–water detonations—I. Model formulation and example results, *Int. J. Heat Mass Transfer* **34**, 2435–2448 (1991).

10. D. F. Fletcher, An improved mathematical model of melt–water detonations—II. A study of escalation, *Int. J. Heat Mass Transfer* **34,** 2449–2459 (1991).
11. W. M. Ren, S. M. Ghiaasiaan and S. I. Abdel-Khalik, GT3F: an implicit finite-difference computer code for transient three-dimensional three-phase flow—I. Governing equations and solution scheme, *Numer. Heat Transfer B* **25,** 1–20 (1994).
12. W. M. Ren, S. M. Ghiaasiaan and S. I. Abdel-Khalik, GT3F: an implicit finite-difference computer code for transient three-dimensional three-phase flow—II. Applications, *Numer. Heat Transfer B* **25,** 21–38 (1994).
13. N. I. Kolev, The code IVA3 for modeling of transient three-phase flows in complicated 3D geometry, *Kernetechnik* **58,** 147–156 (1993).
14. H. B. Stewart and B. Wendorff, Two-phase flow: models and methods, *J. Comput. Phys.* **56,** 363–404 (1984).
15. I. Kataota, M. Ishii and A. Serizawa, Local formulation and measurement of interfacial area concentration in two-phase flow, *Int. J. Multiphase Flow* **12,** 505–529 (1986).
16. J. M. Heuss, C. J. King and C. R. Wilke, Gas–liquid mass transfer in cocurrent froth flow, *A.I.Ch.E. Jl* **11,** 866–873 (1965).
17. D. S. Scott and W. Hayduk, Gas absorption in horizontal cocurrent bubble flow, *Can. J. Chem. Engng* **44,** 130–136 (1966).
18. J. C. Lamont and D. S. Scott, Mass transfer from bubbles in cocurrent flow, *Can. J. Chem. Engng* **44,** 201–208 (1970).
19. J. C. Lamont and D. S. Scott, An eddy cell model of mass transfer into the surface of a turbulent liquid, *A.I.Ch.E. Jl* **16,** 513–519 (1970).
20. J. C. Jepsen, Mass transfer in two-phase flow in horizontal pipelines, *A.I.Ch.E. Jl* **16,** 705–711 (1970).
21. Y. Taitel, D. Bornea and A. E. Dukler, Modeling flow pattern transitions for steady upward gas–liquid flow in vertical tubes, *A.I.Ch.E. Jl* **26,** 345–354 (1980).
22. G. Kasturi and J. B. Stepanek, Two-phase flow—III. Interfacial area in cocurrent gas–liquid flow, *Chem. Engng Sci.* **29,** 713–719 (1974).
23. G. Kasturi and J. B. Stepanek, Two-phase flow—IV. Gas and liquid side mass transfer coefficients, *Chem. Engng Sci.* **29,** 1849–1856 (1974).
24. T. Tomida, M. Yoshida and T. Okazaki, Liquid-side volumetric mass transfer coefficient in upward two-phase flow of air–liquid mixtures, *J. Chem. Engng Japan* **9,** 464–468 (1976).
25. L. G. Neal and S. G. Bankoff, A high resolution resistivity probe for determination of local void properties in gas–liquid flow, *A.I.Ch.E. Jl* **9,** 490–494 (1963).
26. K. Kakizawa and Y. Sakurai, Basic studies on two-phase flow with the use of electrical void-meter, *Nucl. Sci. Technol.* **5,** 153–159 (1968).
27. M. S. Hoffer and W. Resnik, A modified electro-resistivity probe technique for steady- and unsteady-state measurement in fine dispersions—I. Hardware and practical operating aspects, *Chem. Engng Sci.* **30,** 473–480 (1975).
28. J. M. Burgess and P. H. Calderbank, The measurement of bubble parameters in two-phase dispersions—I. The development of an improved probe technique, *Chem. Engng Sci.* **30,** 743–750 (1975).
29. R. Van der Welle, Void fraction, bubble velocity and bubble size in two-phase flow, *Int. J. Multiphase Flow* **11,** 317–345 (1985).
30. G. Kocamustafaogullari and Z. Wang, An experimental study of local interfacial parameters in a horizontal bubbly two-phase flow, *Int. J. Multiphase Flow* **17,** 553–572 (1991).
31. S. T. Revankar and M. Ishii, Theory and measurement of local interfacial area using a four sensor probe in two-phase flow, *Int. J. Heat Mass Transfer* **36,** 2997–3007 (1993).
32. W. Gestrich and W. Krauss, Specific interfacial area in bubble layers, *Int. Chem. Engng* **16,** 10–18 (1976).
33. W. D. Deckwer, I. Alder and A. Zaidi, A comprehensive study on CO_2-interphase mass transfer in vertical cocurrent and countercurrent gas–liquid flow, *Can. J. Chem. Engng* **56,** 43–45 (1978).
34. K. W. Robinson and C. R. Wilke, Simultaneous measurement of interfacial area and mass transfer coefficients for a well-mixed gas dispersion in aqueous electrolyte solutions, *A.I.Ch.E. Jl* **20,** 285–294 (1974).
35. J. Landau, J. Boyle, H. G. Gomaa and A. M. Al Taweel, Comparison of models for measuring interfacial areas in gas–liquid dispersions, *Can. J. Chem. Engng* **55,** 13–18 (1977).
36. T. Sridhar and O. E. Potter, Interfacial area measurements in gas–liquid agitated vessels, *Chem. Engng Sci.* **33,** 1347–1353 (1978).
37. A. M. Al Taweel, R. Divakarla and H. G. Gomaa, Measurement of large gas–liquid interfacial areas, *Can. J. Chem. Engng* **62,** 73–77 (1984).
38. S. Banjeree, D. S. Scott and E. Rhodes, Studies on countercurrent gas–liquid flow in helically coiled tubes, *Can. J. Chem. Engng* **48,** 542–551 (1970).
39. R. V. Shilimkan and J. B. Stepanek, Interfacial area in cocurrent gas–liquid upward flow in tubes of various sizes, *Chem. Engng Sci.* **32,** 149–154 (1977).
40. T. Tomida, F. Yusa and T. Okazaki, Effective interfacial area and liquid-side mass transfer coefficient in upward two-phase flow of gas–liquid mixture, *Chem. Engng Sci.* **16,** 81–88 (1978).
41. A. P. Watson, D. E. Cormack and M. E. Charles, A preliminary study of interfacial areas in vertical cocurrent two-phase flow, *Can. J. Chem. Engng* **57,** 16–23 (1979).
42. J. S. Vavruska and J. J. Perona, Measurement of interfacial areas in cocurrent gas–liquid downward flow, *Can. J. Chem. Engng* **58,** 141–144 (1980).
43. J. M. Dejesus, Measurements of interfacial area and void fraction for two-phase flow in a vertical tube, M.S. Thesis, University of Toronto, Canada (1989).
44. W. K. Lewis and W. G. Whitman, Principle of gas absorption, *Ind. Engng Chem.* **16,** 1215–1220 (1924).
45. R. Higbie, The rate of absorption of a pure gas into a still liquid during short periods of exposure, *Trans. Am. Instn Chem. Engrs* **35,** 365 (1935).
46. P. V. Danckwerts, Significance of liquid-film coefficients in gas absorption, *Ind. Engng Chem.* **43,** 1460–1467 (1951).
47. M. K. Kishinevskii, Two approaches to the theoretical analysis of absorption processes, *J. Appl. Chem. USSR* **28,** 881–886 (1955).
48. G. E. Fortescue and J. R. A. Pearson, On gas absorption into a turbulent liquid, *Chem. Engng Sci.* **22,** 1163–1176 (1967).
49. L. K. Brumfield, R. N. Houze and T. G. Theofanous, Turbulent mass transfer at free, gas–liquid interfaces, with applications to film flows, *Int. J. Heat Mass Transfer* **18,** 1077–1081 (1975).
50. T. G. Theofanous, R. N. Houze and L. K. Brumfield, Turbulent mass transfer at free gas–liquid interfaces, with applications to open-channel, bubble and jet flows, *Int. J. Heat Mass Transfer* **19,** 613–624 (1976).
51. V. G. Levich, *Physicochemical Hydrodynamics*. Prentice-Hall, Englewood Cliffs, NJ (1962).
52. D. K. Edwards, V. I. Denny and A. F. Mills, *Transport Processes* (2nd Edn). McGraw-Hill, New York (1979).
53. H. Hikita, S. Asai and Y. Azuma, Solubility and diffusivity of oxygen in aqueous sucrose solutions, *Can. J. Chem. Engng* **56,** 371–374 (1978).
54. M. K. Chaudhury and R. J. Good, A quantitative theory of negative absorption of nonelectrolytes caused by repulsive van der Waals forces, *Langmuir* **1,** 673–678 (1985).

55. D. Luo, Interphase transfer process in cocurrent two-phase channel flow, Ph.D. Dissertation, G. W. Woodruff School of Mechanical Engineering, Georgia Institute of Technology, Atlanta, GA (1995).
56. D. J. Nicklin, J. O. Wilkes and J. F. Wilkes, Two-phase flow in vertical tubes, *Trans. Instn Chem. Engrs* **40,** 61–68 (1962).
57. G. W. Govier and K. Aziz, *The Flow of Complex Mixtures in Pipes*. Robert E. Krieger, Malabar, FL (1972).
58. G. B. Wallis, *One-dimensional Two-Phase Flow*. McGraw-Hill, New York (1969).
59. S. M. Ghiaasiaan, K. E. Taylor, B. K. Kamboj and S. I. Abdel-Khalik, Countercurrent two-phase flow regimes and void fractions in vertical and inclined channels, *Nucl. Sci. Engng* **119,** 182–194 (1995).
60. C. S. Martin, Vertical downward two-phase slug flow, *J. Fluids Engng* **98,** 715–722 (1976).